

Review paper: The 20th May 2016 M_w 6.1 Petermann surface rupturing earthquake, Australia

Tamarah King

School of Earth Sciences, The University of Melbourne, Victoria 3010, Australia
tamarah.king@unimelb.edu.au
<https://orcid.org/0000-0002-9654-2917>

Mark Quigley

School of Earth Sciences, The University of Melbourne, Victoria 3010, Australia
Mark.quigley@unimelb.edu.au
<https://orcid.org/0000-0002-4430-4212>

Dan Clark

Geoscience Australia, Canberra 2601, Australia
<https://orcid.org/0000-0001-5387-4404>

Abstract

The 20th May 2016 M_w 6.1 Petermann earthquake produced a 21 km long surface rupture with a maximum vertical offset of 0.9 m. Geological and geophysical data provide strong evidence that rupture occurred along a mylonite foliation plane with an orientation defined by deformation from the nearby Woodroffe Thrust, a major Neoproterozoic terrane suture. The most geologically and seismologically reasonable fault model involves 2 bedrock-controlled faults with slightly oblique orientations. In this model, rupture propagates from a hypocentre at ≤ 4 km depth, with a centroid of slip located at the inferred intersection of the two faults at 1 km depth. No evidence of prior rupture has been identified in the landscape or in shallow trenches crossing the rupture.

This document presents a review of available literature related to the 2016 Petermann surface rupturing earthquake. It includes newly digitised data related to the rupture and new interpretations of controls on fault rupture. It supplements a manuscript reviewing all Australian surface rupturing earthquakes, submitted to Geosciences in August 2019.

Please contact authors on the content presented herein; we welcome constructive feedback.

1. Geology

1.1 Regional / background

The 2016 Petermann, 2012 Pukatja and 1986 Marryat Creek surface rupturing earthquakes occurred within the Musgrave Block, a Mesoproterozoic basement assemblage that extends across the Northern Territory / South Australia border into Western Australia (Figure 1). This block is composed of high grade metamorphic and magmatic suites formed during the ~1200 Ma Musgrave orogen and reworked during the 580 - 520 Ma Petermann Orogeny (Aitken and Betts, 2009; Cawood and Korsch, 2008; Edgoose et al., 2004; Raimondo et al., 2010). Two large structures, the Woodroffe Thrust and Mann Fault, dominated uplift and deformation during the Petermann Orogeny (Lambeck and Burgess, 1992; Neumann, 2013; Stewart, 1995; Wex et al., 2019). The Woodroffe Thrust was responsible for significant exhumation of lower-crustal rocks, displacing the Moho by ~20 km associated with a present-day large gravitational and magnetic anomaly (Hand and Sandiford, 1999; Korsch et al., 1998; Wade et al., 2008). The Petermann and Pukatja surface ruptures occurred within 10 km of the Woodroffe Thrust (on the hanging-wall).

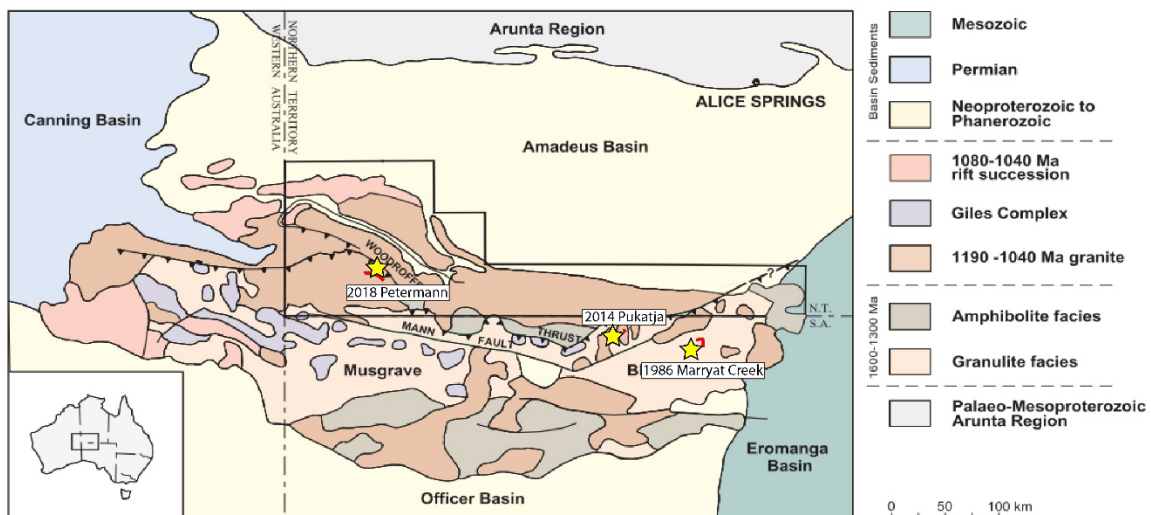


Figure 1: Musgrave Block geology from Figure 3 of Edgoose et al. (2004) with Petermann, Pukatja and Marryat Creek earthquakes (yellow star) and ruptures (red lines) overlaid. Note some authors locate the Mann Fault further south than this map, coincident with the location of the Marryat Creek rupture (Aitken and Betts, 2009; Raimondo et al., 2010). (CC) NT Gov.

1.2 Local units / bedrock

Isolated small (~ 0.5 – 5 m diameter) and low-lying (< 1 m height) granitic mylonite outcrops occur along four segments of scarp, including three instances of rupture over/against footwall bedrock (Figure 2) with the same strike and dip of rupture. Mylonite foliations of outcrops within 3 km of the rupture on both the hanging-wall and foot-wall align in the same direction as rupture (striking NW, dipping NE) (Figure 3).



Figure 2: Image of the Petermann scarp where it ruptures over mylonitic bedrock (King et al., 2018)

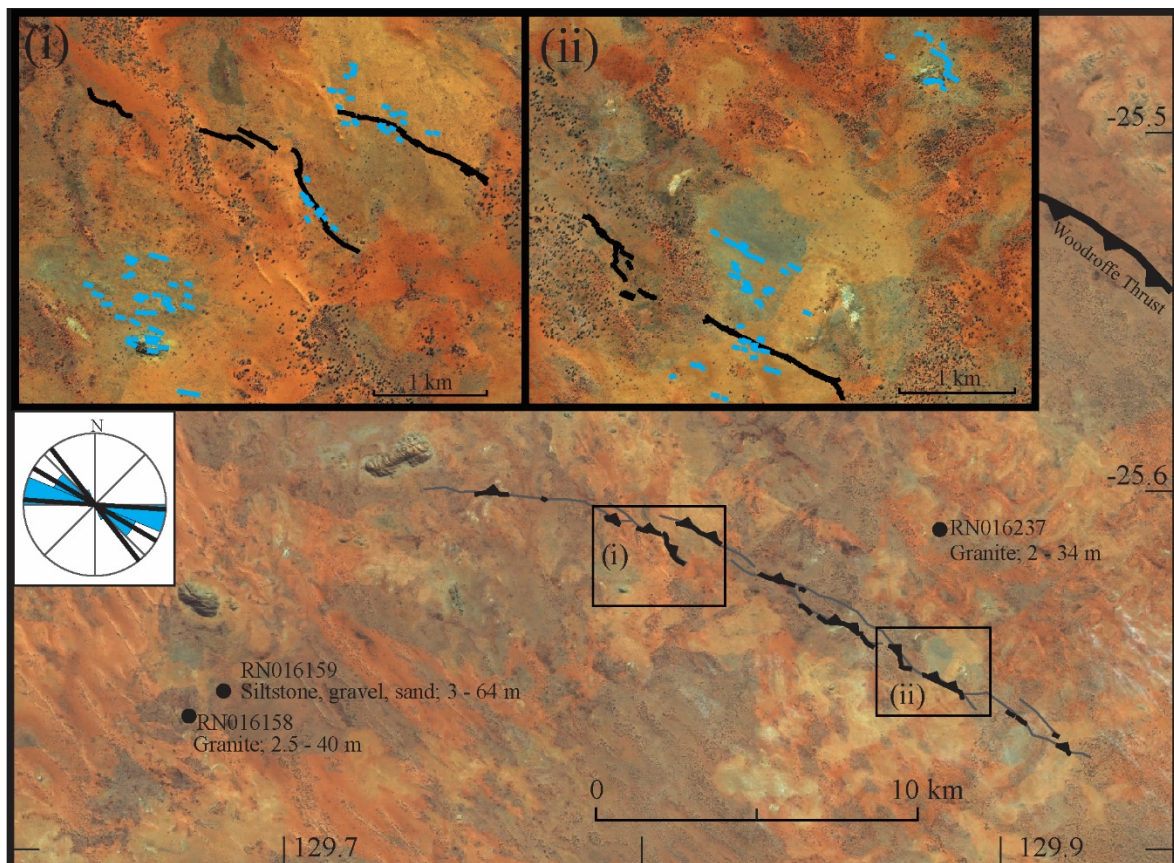


Figure 3: Satellite imagery (Bing © 2019 DigitalGlobe, HERE, Microsoft) showing Petermann surface rupture (black) and InSAR trace (grey) with locations of bores showing shallow granitic bedrock (< 2.5 m) across the area, and insets (i) and (ii) showing mylonite bedrock orientations in the vicinity of surface rupture strands.

Isolated larger (50 – 200 m diameter, 1 – 15 m height) granite outcrops occur across the area within 200 m of the rupture (Figure 3, Figure 5). These represent areas of low-shear within the mylonite unit, which preserve isolated unfoliated granite protolith. This includes Duffield Rocks and Mount Jenkins at the NW of the scarp, significant outcrops of 100 m elevation. No direct observations exist of these outcrops as they are places of cultural significance.

The Woodroffe Thrust is mapped approximately 10 km to the NE based on geophysical data (Edgoose et al., 2004; Scrimgeour et al., 1999a). The fault does not outcrop in this region of the Musgrave Block. Seismic reflection data (Neumann, 2013) from ~200 km west suggest the Woodroffe Thrust in this area has a dip of 30° ($\pm \sim 10^\circ$) and may be 3 km wide (Raimondo et al., 2010). The Woodroffe Thrust is visible in magnetic and gravity data (*Figure 4*), and the heavily deformed mylonites on the hanging-wall are clearly visible as linear magnetic anomalies. The historic surface rupture location and orientation align with these linear magnetic anomalies, and the edge of the Woodroffe Thrust gravity anomaly (*Figure 4*).

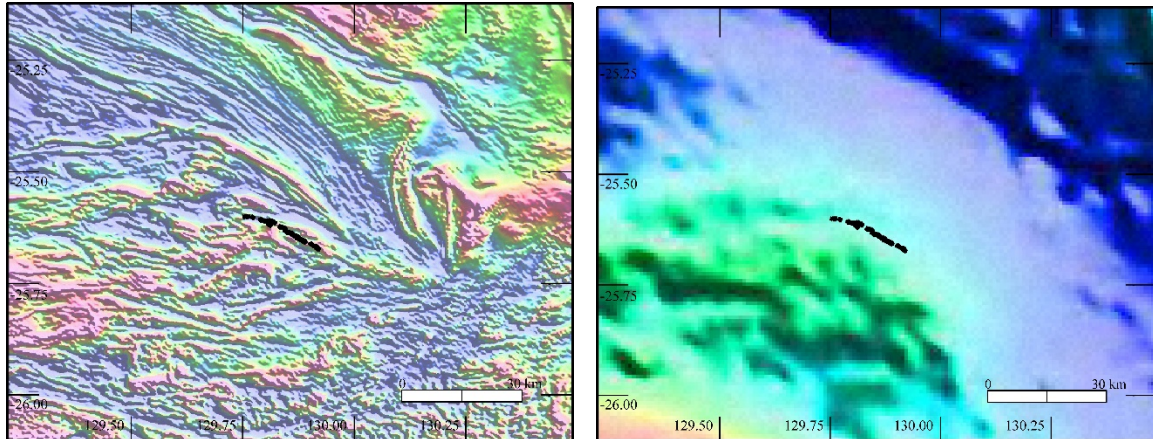


Figure 4: Petermann scarp (black lines) relative to magnetic intensity and bouguer gravity anomaly maps. National bouguer gravity anomaly map: <http://pid.geoscience.gov.au/dataset/ga/101104>; National total magnetic intensity map: <http://pid.geoscience.gov.au/dataset/ga/89596>

1.3 Surficial deposits

Stable Pleistocene sand dunes up to 8 m high aligned NE-SW cover the area. Colluvium and calcrete exist in the inter-dune areas between, and covering, bedrock outcrops (*Figure 5*).

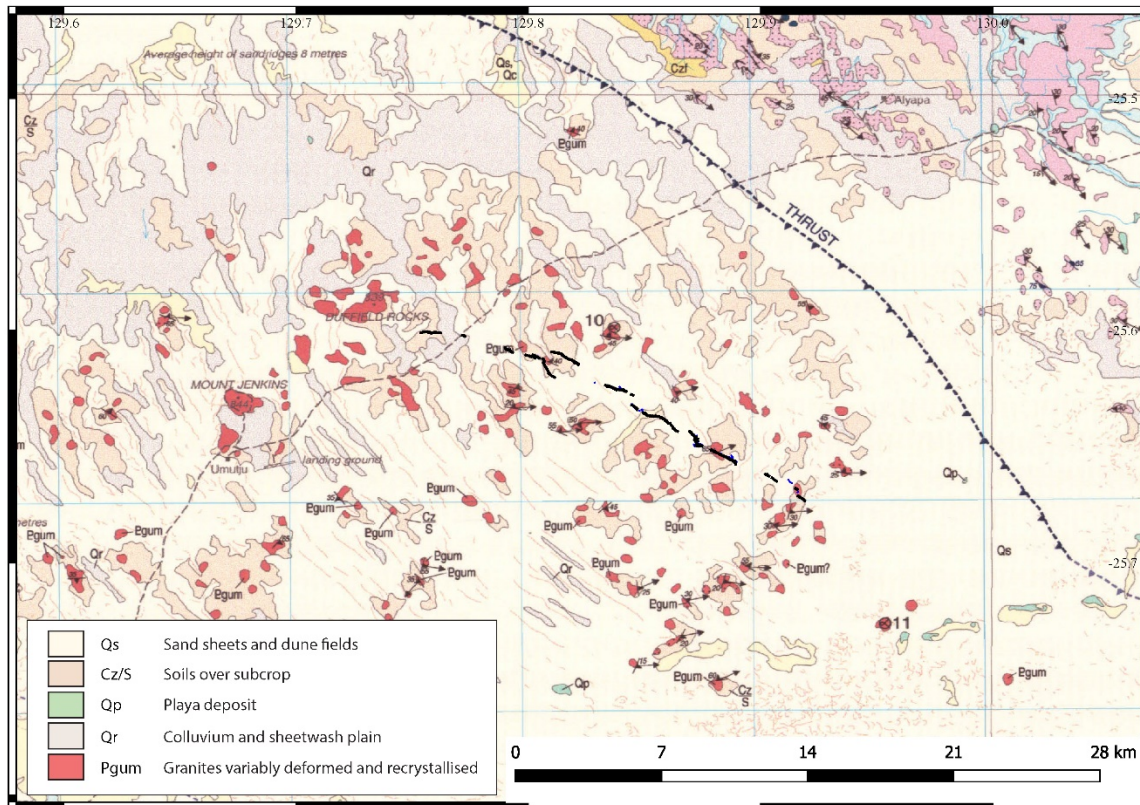


Figure 5: Crop of Petermann 1:250 000 geological map sheet (Scrimgeour et al., 1999b) showing basement and surface sediments around the Petermann surface rupture. Full map and legend available from: <https://geoscience.nt.gov.au/gemis/>, (CC) NT Gov.

2. Seismology

2.1 Epicentre and magnitude

Table 1 and Figure 6 show four online published epicentre locations for the Petermann earthquake. Hejrani and Tkalčić (2018) also derive a centroid location using investigation of full waveform data, which is located 1.5 km west of the GA epicentre. It is not clear whether seismic waveforms or source modelling from InSAR data were used in the Polcari et al. (2018) epicentre solution. Maps of this paper show the epicentre located ~ 5 km north of the epicentre described by easting and northing coordinates for their seismic source (Table 1 of that paper, reproduced in Table 1 and Figure 6 below). All epicentre locations are within a 5 km radius of each other on the hanging-wall of the surface rupture. Statistical uncertainties (precision) for the USGS epicentre (± 2.2 km) may not capture epistemic uncertainties introduced by the distance between the epicentre and closest seismometer (~ 166 km). Uncertainties reported by GA ($\pm 6 - 8$ km) are closer to estimates for historic remote earthquakes (e.g. ± 10 km (Leonard, 2008)). The Petermann earthquake is the only historic Australian surface rupturing earthquakes for which initial epicentre solutions lie on the hanging-wall of the surface rupture, at a distance that is geologically reasonable to produce the surface rupture.

Table 1 : Published epicentre locations, depths and magnitudes

Reference	Agency	Latitude	\pm (km)	Longitude	\pm (km)	Depth (km)	\pm (km)	M1	M2	M3
King et al (2018)	GA	-25.579	8.77	129.832	6.12	0		6.09 Mw	6.14 ML	6.38 Ms

King et al (2018)	GCMT	-25.61		129.94									
King et al (2018)	Geofon	-25.62		129.88									
King et al (2018)	USGS	-25.566	2.2	129.884	2.2	10	1.7	6	Mw	6.1	ML	6.2	Ms
Polcari et al (2018)		-25.6177	0.57	129.865	0.95			6.06	?				
Hejrani et al (2019)	(centroid)	-25.6		129.8		1		5.9	Mw				

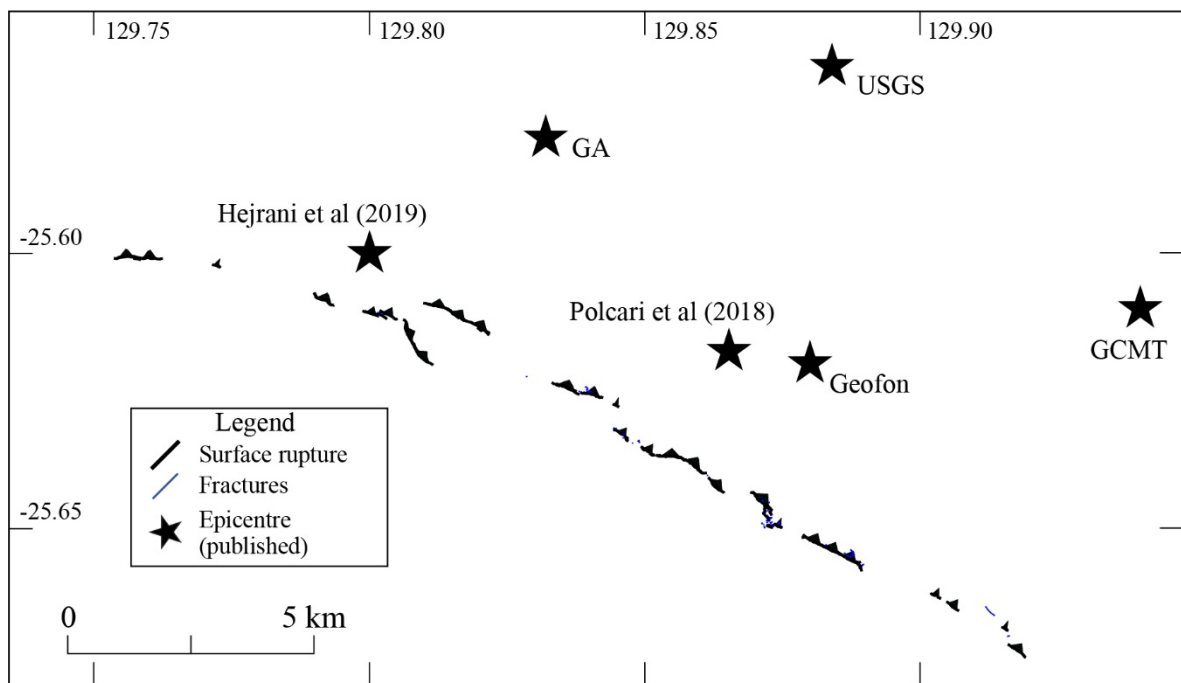


Figure 6: Published epicentre locations around the surface rupture

This paper prefers the magnitude (M_w 6.1) of Geoscience Australia. Modelling of slip from InSAR (Polcari et al., 2018) and modelling of full waveform data using a 3D Australian crustal model (Hejrani and Tkalčić, 2018) result in magnitude values close to the USGS magnitude (M_w) and likely within error of each other (5.9 – 6.06, Table 1).

2.2 Focal mechanisms

Six focal mechanisms have been published (Figure 7), all consistent with predominately reverse movement trending NW-SE. Four solutions show a minor component of sinistral movement on the NE dipping plane, which is the preferred solution based on surface rupture orientation. Hejrani and Tkalčić (2018) derive a centroid of slip solution by modelling synthetic waveforms through a 3D earth model of the Australian crust, to compare to full waveform data for the earthquake from four Australian stations. The IGP solution uses teleseismic P- and S- body waves, while the Polcari et al. (2018) solution appears to be derived from best-fit parameters from inversion models describing InSAR data.

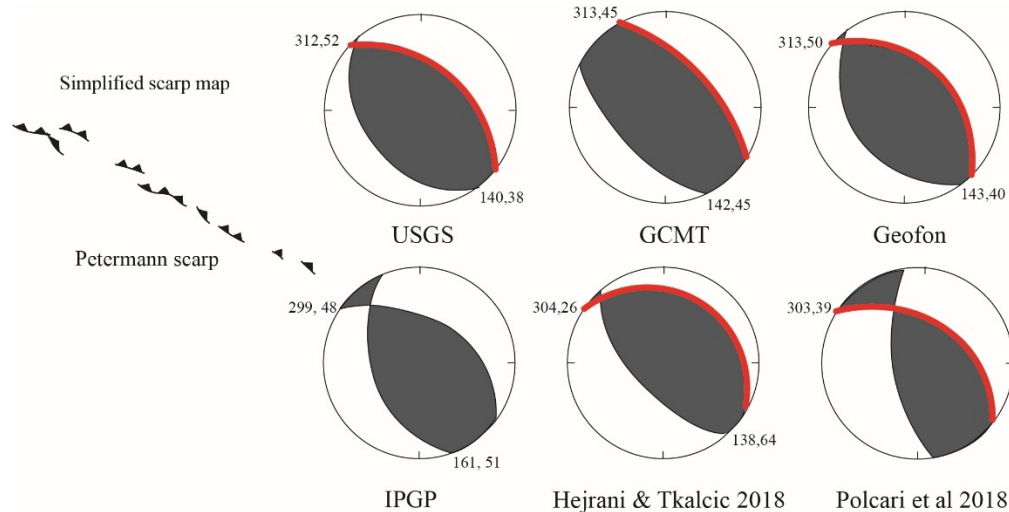


Figure 7: Published focal mechanism and simplified scarp map

2.3 Depth

Depth estimates from GA, USGS and CMT fall between 7 – 12 km, though the USGS also publish a 2 km depth based on body-wave moment tensor results. From inversion of InSAR data, Polcari et al. (2018) derive a depth to the top of the fault plane of 450 m. This would imply the fault is blind, despite discrete surface rupture being observed. Hejrani and Tkalčić (2018) resolve a centroid depth of 1 km, but suggest the distance to the closest seismometer (~166 west) restricts the ability to obtain a hypocentral depth. They apply empirical magnitude and rupture area relationships from Somerville et al. (1999) to derive a 4 km wide fault with a ~ 90 km² fault area. Fault rupture of < 4 km depth is consistent with their 1 km centroid depth. Wang et al. (2019) use a strike-variable fault model to derive source parameters from InSAR data, and find slip concentrated between 0 and 3 km depth.

2.4 Foreshock / aftershocks

The day before the mainshock, a M_L 3.5 was recorded by GA 2 km N of the surface rupture and 5 km W of the mainshock location (± 12 km). Prior seismicity within a 30 km radius includes four M_L 3.2 - 4.4 events between 1986 - 1993, 24 – 27 km north of the epicentre. It is estimated that the GA catalogue is complete for $M_L > 3.5$ by ~1980 (Leonard, 2008) however epicentres in this remote area have large epistemic uncertainties resulting in inaccurate locations. This is exemplified by mislocation of the 2012 Pukajta earthquake epicentre 17 km away from the surface rupture location, and the 1986 Musgrave earthquake 30 km away from its surface rupture.

A temporary seismometer array was deployed by GA within 3 days of the mainshock, with extra seismometers added to the network by University of Melbourne seismologists approximately two weeks later. For the 15 months that this array was deployed and active, hundreds of aftershocks were recorded, though only 143 have been located to date. Of those located aftershocks, 65 have depths, shown in Figure 1 of King et al. (2018). These project to a 2D plane dipping 10° - 30° that does not project to the surface at the location of surface rupture. This may be due to (a) mainshock rupture propagating along the plane defined by aftershocks but changing to a different plane in the near-surface, producing the surface rupture at that location (b) rupture propagating upwards along the plane defined by aftershocks with the plane significantly steepening close to the surface rupture (c) aftershocks do not define the mainshock fault plane, but represent redistribution of stress on adjacent foliation planes (d) aftershocks occurred on multiple planes that are not well imaged when aftershocks are projected to a 2D plane. Available aftershock data may be affected by selection bias, as not all of the data from the temporary seismometer array has been processed yet.

3. Surface Rupture

3.1 Authors / map quality

The Petermann surface rupture occurred 156 km away from Yulara (Uluru) with access via a dirt track which runs between Yulara and the APY lands near the NT/SA/WA border. The area is protected under the Indigenous land rights act. At the time of writing, one paper has been published on ground observations from the Petermann earthquake (King et al., 2018), and one of InSAR deformation defining a surface rupture (Polcari et al., 2018). Gold et al. (2017) describes a Worldview (c) satellite derived surface rupture trace, this data is currently in review for publication.

3.2 Length and shape

The Petermann surface rupture was mapped by field work, satellite and drone imagery (*Figure 8a*) defining a 20.3 km long rupture from tip to tip along a simplified trace (*Figure 8b*). The scarp consists of two main rupture strands with a 1.2 km long overlap ~ 8 km from its north-western most tip which define a slightly convex shape (relative to the hanging-wall). The distance between scarp strands at this step over is 0.6 – 0.8 km. The visible rupture trace is highly discontinuous relative to the trace defined by InSAR (*Figure 8a*). The trace of InSAR displacement also extends 1.4 km longer than visible rupture at the north-western end and 0.6 km longer at the south-eastern end (*Figure 8a*). The InSAR length end to end along a simplified trace is 22.6 km (*Figure 8b*), 10% longer than the visible rupture simplified length.

Applying a criteria which simplifies ruptures to straight traces and defines distinct faults where mapped primary rupture has gaps/steps > 1 km and/or where strike changes by $> 20^\circ$ for distances > 1 km (c.f., (Quigley et al., 2017)) results in three faults for visible rupture length with a sum length of 21 km, and two faults for InSAR with a sum length of 21.5 km (*Figure 8c*). The specified criteria separate the north-western strand of visible rupture into two faults with a short 1 km section at the location of step-over, due to an inter-rupture angle $> 20^\circ$. We prefer a fault model where this section is a single fault based on the InSAR trace and the length of this segment which only just reaches the criteria (1.02 km). In our preferred model, the Petermann rupture defines two faults with a sum length of 21 km.

Figure 8d maps portions of the scarp where more than two vertical displacement measurements of greater than 0.2 m occur within a distance of 1 km (data from Attanayake et al. (2019) and Gold et al. (2019) in review). Applying cosmogenic erosion rates from lithologically and climatically analogous settings of Australia (0.3 – 5 m/Myr; Bierman and Caffee, 2002) suggests that 0.2 m of scarp height could be removed within 35 – 660 kyrs, leaving ~ 12.2 km of rupture length visible in the landscape (this is a sum length of four discontinuous rupture traces which show offsets > 0.2 m) (*Figure 8d*). This suggests that the surface scarp may not persist within this landscape as a mappable scarp, unless recurrence intervals are < 0.5 to 1 Myr. Due to the climate and geography of the rupture location, we prefer a degradation rate on the longer end of this range. In this calculation we assume that the scarp is shallowly underlain by granitic bedrock and that the scarp erodes more rapidly than the surrounding terrain at rates commensurate with Bierman and Caffee (2002). We do not account for erosion rates of any duricrust which may overlie granitic bedrock or anthropogenically- and/or climatically-modulated variations in erosion rates.

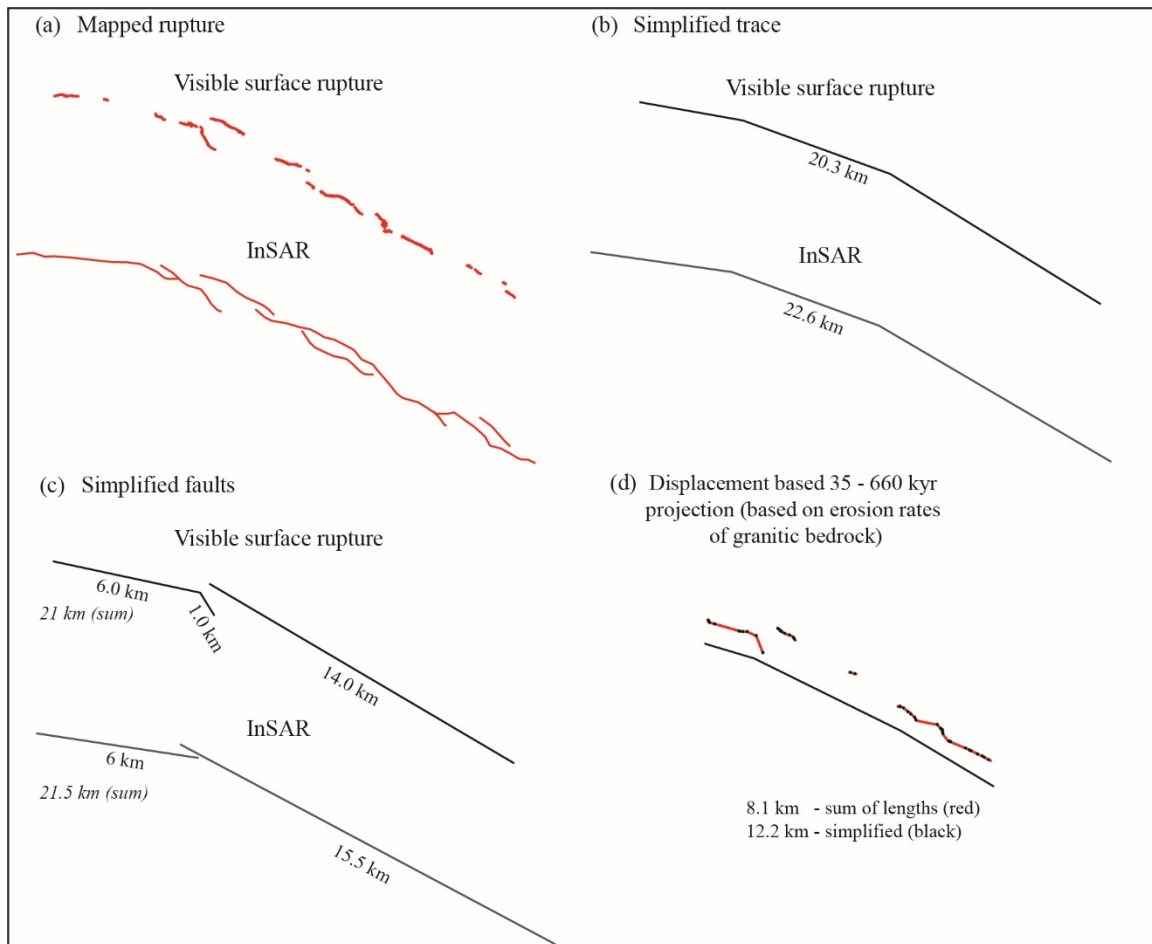


Figure 8; Measures of length for the Petermann rupture as described in the text

3.3 Strike

Focal mechanisms derived for this event show strikes ranging from 299° to 313° , with best fits of InSAR and waveform inversion of 303° to 304° from Polcari et al. (2018) and Hejrani and Tkalčić (2018). The average strike of rupture as measured from the tips of the InSAR derived trace is 294° (this does not account for rupture curvature). The north-western fault defined in Figure 8c is 280° while the south-eastern fault is 298° .

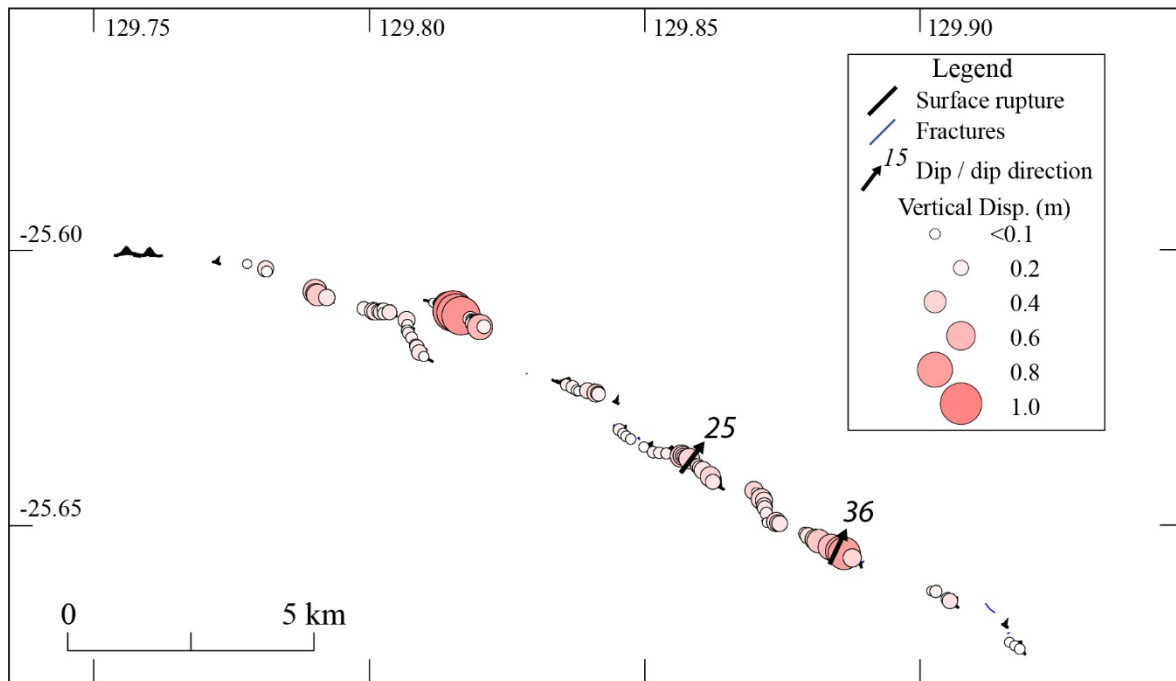


Figure 9: Map of the Petermann visible surface rupture, fractures (most are within 100m of rupture and not visible at this map scale), vertical offset measurements ((Attanayake et al., 2019) in review), and dip measurements from trenching (unpublished data).

3.4 Dip

Unpublished field data from two small hand-dug trenches across the Petermann scarp show dips of 25° where rupture runs through calcrete and sand in an inter-dune palaeovalley (e.g. Magee (2009)), and 36° across an inter-dune region where rupture is within 5 m of bedrock outcrops.

Focal mechanisms from the USGS, GCMT, Geofon and IGP range from $48^\circ - 52^\circ$ for the northeast dipping plane. Hejrani and Tkalčić (2018) derive a centroid of slip focal mechanism with a dip of $26^\circ \pm 4^\circ$ using full waveform data and an Australian specific 3D earth model. Polcari et al. (2018) derive a focal mechanism with a 39° NE dipping plane from InSAR inversion modelling. Wang et al. (2019) suggest that the InSAR modelling results of Polcari et al. (2018) are inaccurate due to a fixed strike fault model. They use a variable strike fault model in their InSAR inversion modelling and find an optimal dip of 22° NE.

Aftershocks define a plane dipping $10^\circ - 30^\circ$ that does not intersect with surface rupture, or a dip of $30^\circ - 40^\circ$ if the plane defined by aftershocks is forced to intersect with the surface rupture.

3.5 Morphology

As described in King et al. (2018), offset of the hanging-wall relative to the footwall was observable as discrete rupture, mole tracks (Figure 10a) and warping or folding of the hanging-wall sediments over the footwall sediments (e.g. Figure 4 of King et al. (2018)). Rupture is discontinuous in the field with variable strike and morphology on a smaller scale (i.e. $10^0 - 10^1$ m). Discrete rupture was observed to progress into gentle warping or mole-tracks at the ends of segments, often terminating at the edges of sand dunes (Figure 10c). Figure 4 of King et al. (2018) shows duplexing discrete ruptures stepping backwards on the hanging-wall, with most offset captured by the furthest strand (relative to the hanging-wall). Discrete rupture was also evident as rupture steps with limited overlap of sections (Figure 10b) separated by ramps. Where rupture passed through significant sand dunes (Figure 10c) it became difficult to see in the field and optical imagery (satellite, drone) (King et al., 2018). InSAR shows vertical offsets near the NW end of rupture that are not visible in the field, potentially due to

deformation being distributed across a broader area (e.g. tens to hundreds of meters) rather than a discrete scarp.

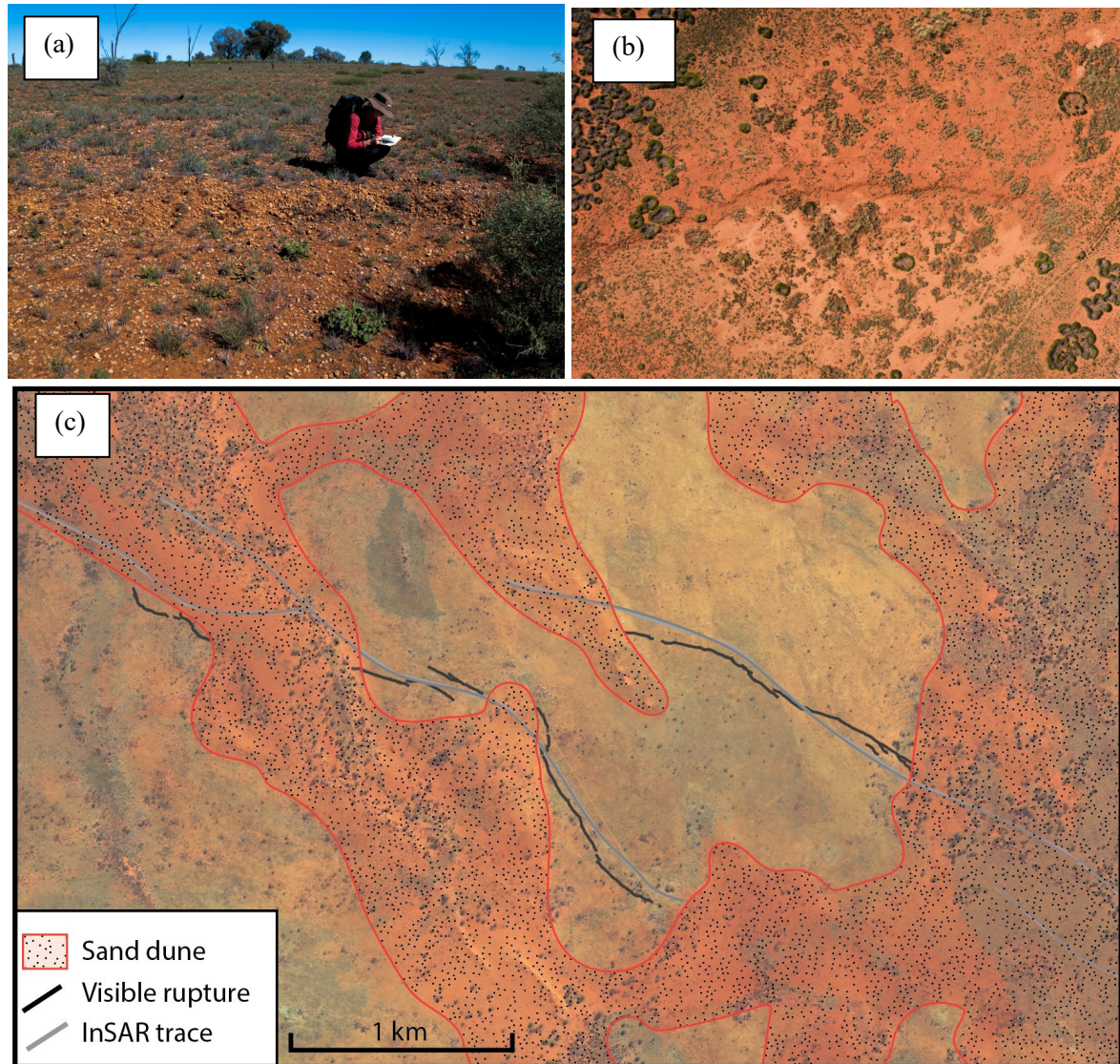


Figure 10: Images of the Petermann scarp where (a) scarp consists of moletrack style rupture through loose calcrete and sand (b) drone-derived imagery showing 5 – 10 m left stepping rupture connected by ramps (c) satellite view (Bing © 2019 DigitalGlobe, HERE, Microsoft) showing effect of sand dunes on visible surface rupture trace relative to InSAR trace.

3.6 Lateral offsets

No detailed analysis of kinematics based on surface observations has been published, though three of five focal mechanisms show a minor sinistral component. The only linear features crossing the scarp are a single camel track (Figure 11) and the vehicle track in the NW, neither of which had observable lateral offsets.



Figure 11: Image of a camel track that crosses the Petermann scarp, the only linear feature offset by rupture, which shows no clear sign of lateral displacement

3.7 Displacement

King et al. (2018) describe highly variable vertical offset along the visible surface rupture traces, with offset measurements from 0.05 -0.9 m shown in Figure 4 (measured with an RTK GPS). The Gold et al. (2017) abstract describes vertical offsets between 0.2 - 0.6 m using pre- and post- event digital terrain models derived from Worldview satellite imagery. Unlike the RTK measurements which record offset only at the surface rupture interface, the satellite data show vertical offsets across 0.1 – 1 km lengths across the rupture, and therefore capture some distributed deformation.

ALOS-2 ascending wrapped interferograms and displacement maps show ~60 cm of displacement on the hanging-wall and ~12 cm displacement on the footwall (Polcari et al., 2018) while the Sentinel-1 descending data show 13 cm hanging-wall, and 6 cm footwall displacement. The differences in these measures derive from the different line of sights (LOS) for the satellites with the ALOS-2 LOS ~140° from the rupture (almost perpendicular) and Sentinel-1 LOS ~10° from the rupture (almost parallel). Displacements measured by InSAR show a combined vertical, lateral and heave measurement. InSAR shows that displacement extends for ~7 km on the hanging-wall and ~3 km on the footwall away from the surface rupture itself. No hanging-wall depression is evident in the InSAR data, with the Woodroffe Thrust potentially acting as a structural impediment to hanging-wall bending.

Analysis of surveyed offsets along the rupture, and InSAR / satellite derived offsets are currently in review (Attanayake et al., 2019; Gold et al., 2019). Data from RTK measurements along the rupture are shown in Figure 12.

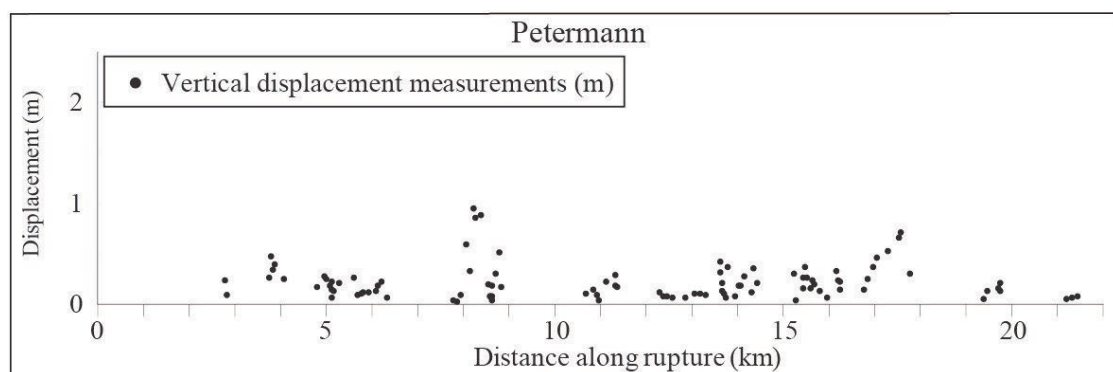


Figure 12: Vertical displacement measurements along the Petermann scarp (published in (Attanayake et al., 2019) and (Gold et al., 2019) (both in review))

3.8 Environmental damage

King et al. (2018) describe environmental damage from the Petermann earthquake in detail, including an isoseismal map (*Figure 13*) based on the Environmental Seismic Intensity scale (ESI-07) (Michetti et al., 2007). Damage is seen to increase towards the surface rupture and is more extensive on the hanging-wall than the footwall. Observed damage includes fissures, surface cracking, fallen trees and limbs, trees killed through root-tear along the hanging-wall, holes in the soil close to the surface rupture, minor rock falls and displaced rock chips.

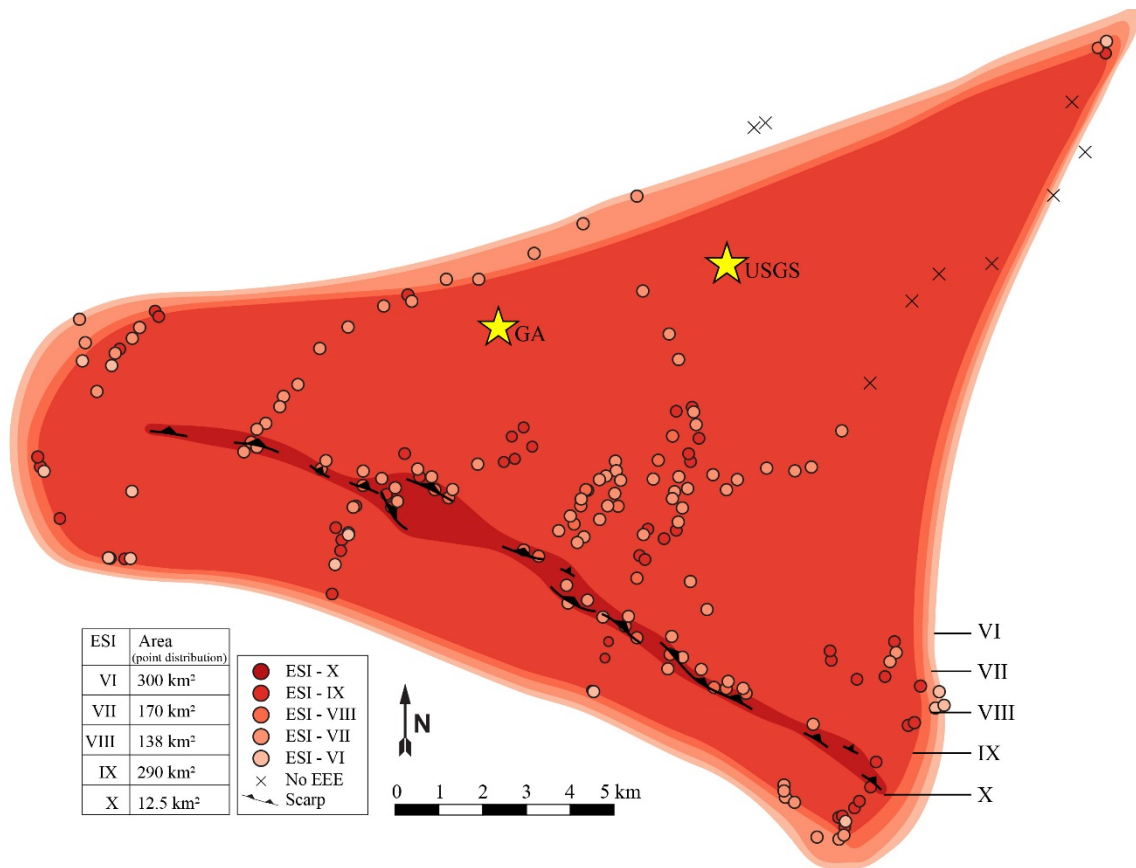


Figure 11
Environmental Seismic Intensity contour map of observed EEEs. Individual data locations have been combined and data along the surface rupture has been removed to enhance visual clarity, these data are included in Figure 1. Some relevant data points where no EEEs were observed are included

Figure 13: Environmental seismic intensity map of the Petermann rupture from King et al. (2018)

4. Paleoseismology

No papers have explored the palaeoseismicity of the Petermann earthquake or surface rupture. There is no topographic or geomorphic evidence of prior rupture along the Petermann scarp within the time constraints imposed by erosion rates of $< 5 \text{ m / Myr}$ (Bierman and Caffee, 2002) (Section 3.2.1). Two hand dug trenches across the rupture (unpublished data) found no displacement of the calcrete underlying eolian sediments. Calcrete in this area is thought to date from wetter conditions potentially during the last glacial maximum (dated at $\sim 8 - 17 \text{ ka}$ in Australia) (Denniston et al., 2013; Field et al., 2017).

4.1 Slip rate

No topographic evidence exists to suggest prior rupture along the Petermann scarp, and no evidence of prior rupture was observed in shallow hand-dug trenches (unpublished field data). The rupture is either the first event on this fault (previously a foliation plane), or the recurrence interval is sufficiently long that all relief relating to prior event(s) was eroded prior to the formation of calcrete exposed in trenches, and deposition of overlying eolian sediment. If recurrence is assumed, vertical

relief generation rates are limited by very low bedrock erosion rates of < 5 m/Myr (Belton et al., 2004; Bierman and Caffee, 2002) (*Figure 8*).

5. Summary

5.1 Surface rupture relationship to Geology

All available evidence suggests that the Petermann earthquake ruptured along a mylonite foliation plane with an orientation related to Woodroffe Thrust deformation. Geophysical data and geological mapping

(King et al., 2018; Scrimgeour et al., 1999b) show the Woodroffe Thrust hanging-wall in this location is composed of metamorphosed granite heavily deformed into mylonite except in isolated larger outcrops of low shear where granitic textures are retained. Where dip is measurable in outcrop, the mylonite dips NE towards the SW dipping Woodroffe Thrust. In multiple locations the surface rupture is coincident with mylonite outcrops on the hanging-wall and foot-wall within 0 – 1 km of the scarp. Surface rupture is observed to rupture against and over outcrops of mylonite with the same strike and dip as the rupture (King et al., 2018). Surface rupture measurements and seismologically derived source parameters show that the earthquake ruptured a plane dipping in a conjugate sense to the SE dipping Woodroffe Thrust (Hejrani and Tkalčić, 2018; King et al., 2018; Polcari et al., 2018).

5.2 Surface rupture relationship to Seismology

The strike of the longest south-eastern section of rupture matches best with waveform modelling and InSAR derived strikes of 303° to 304° (Hejrani and Tkalčić, 2018; Polcari et al., 2018). Maximum vertical offsets are observed at the north-western end (where the scarp step-over occurs) and mid-section of this rupture segment (*Figure 9*). In comparison, the north-western section of rupture is not visible in the field along much of its length due to distributed deformation rather than discrete rupture. This may imply that the south-western segment hosted the majority of seismic slip and moment release, before rupture propagated onto a second fault at the location of scarp stepover. This theory is further supported by the centroid location and depth obtained by Hejrani and Tkalčić (2018) in close proximity to the step-over, potentially related to rupture propagating onto a second fault with a similar but slightly oblique orientation.

Polcari et al. (2018) derive a fault length of 11 km and width of 4 km from InSAR inversion modelling, which does not match with observed rupture length of 21 km. Hejrani and Tkalčić (2018) suggest fault dimensions of 20 km (L) x 4 km (W) based on their derived magnitude value. Aftershock data with well constrained depth measurements show a tight cluster from 2 – 3 km depth and 0 – 4 km ground distance from the rupture. Aftershocks beyond 4 km have a greater range of depth values with a less well-defined planar structure. This may be influenced by selection bias as not all of the aftershock data has been processed to date, and interpretation of the data would be improved by a 3D analysis of aftershock distributions. Despite these uncertainties, the data appear to support a roughly 4 km wide fault plane down to ~ 3 km depth, in line with the Hejrani and Tkalčić (2018) solution.

Acknowledgements

This research was funded by the Australian Research Council through Discovery Grant #DP170103350. T. King received funding through the Australian Government Research Training Program Scholarship. We would like to acknowledge the Pitjantjatjara people of the APY lands in South Australia / Northern Territory, as the traditional custodians of the land on which this surface rupture occurred, and where the data described in this paper were collected. The authors declare no conflict of interest.

6. References

- Aitken, A., Betts, P.G., 2009. Constraints on the Proterozoic supercontinent cycle from the structural evolution of the south-central Musgrave Province, central Australia. *Precambrian Res.* 168, 284–300. <https://doi.org/10.1016/j.precamres.2008.10.006>
- Attanayake, J., King, T.R., Quigley, M.C., Gibson, G., Clark, D., Jones, A., Sandiford, M., 2019. Rupture Characteristics and the Structural Control of the 2016 Mw 6.1 Intraplate Earthquake in the Petermann Ranges, Australia. *Bull. Seismol. Soc. Am.*
- Belton, D.X., Brown, R.W., Kohn, B.P., Fink, D., Farley, K.A., 2004. Quantitative resolution of the debate over antiquity of the central Australian landscape: Implications for the tectonic and geomorphic stability of cratonic interiors. *Earth Planet. Sci. Lett.* 219, 21–34. [https://doi.org/10.1016/S0012-821X\(03\)00705-2](https://doi.org/10.1016/S0012-821X(03)00705-2)
- Bierman, P.R., Caffee, M.W., 2002. Cosmogenic exposure and erosion history of Australian bedrock landforms. *Bull. Geol. Soc. Am.* 114, 787–803. [https://doi.org/10.1130/0016-7606\(2002\)114<0787:CEAEHO>2.0.CO;2](https://doi.org/10.1130/0016-7606(2002)114<0787:CEAEHO>2.0.CO;2)
- Cawood, P.A., Korsch, R.J., 2008. Assembling Australia: Proterozoic building of a continent. *Precambrian Res.* 166, 1–35. <https://doi.org/10.1016/j.precamres.2008.08.006>
- Denniston, R.F., Asmerom, Y., Lachniet, M., Polyak, V.J., Hope, P., An, N., Rodzinyak, K., Humphreys, W.F., 2013. A Last Glacial Maximum through middle Holocene stalagmite record of coastal Western Australia climate. *Quat. Sci. Rev.* 77, 101–112. <https://doi.org/10.1016/j.quascirev.2013.07.002>
- Edgoose, C.J., Scrimgeour, I.R., Close, D.F., 2004. Geology of the Musgrave Block, Northern Territory (NTGS Report 15). Northern Territory Geological Survey, Darwin, Australia.
- Field, E., McGowan, H.A., Moss, P.T., Marx, S.K., 2017. A late Quaternary record of monsoon variability in the northwest Kimberley, Australia. *Quat. Int.* 449, 119–135. <https://doi.org/10.1016/j.quaint.2017.02.019>
- Gold, R., Clark, D., King, T., Quigley, M., 2017. Surface rupture and vertical deformation associated with 20 May 2016 M6 Petermann Ranges earthquake, Northern Territory, Australia, in: European Geosciences Union General Assembly 2017. Vienna, Austria. <https://doi.org/http://adsabs.harvard.edu/abs/2017EGUGA..19.8645G>
- Gold, R.D., Clark, D., Barnhart, W.D., King, T., Quigley, M., Briggs, R.W., 2019. Surface rupture and distributed deformation revealed by optical satellite imagery: The intraplate 2016 Mw 6.0 Petermann Ranges earthquake, Australia. *Geophys. Res. Lett.*
- Hand, M., Sandiford, M., 1999. Intraplate deformation in central Australia, the link between subsidence and fault reactivation. *Tectonophysics* 305, 121–140. [https://doi.org/10.1016/S0040-1951\(99\)00009-8](https://doi.org/10.1016/S0040-1951(99)00009-8)
- Hejrani, B., Tkalčić, H., 2018. The 20 May 2016 Petermann Ranges earthquake: centroid location, magnitude and focal mechanism from full waveform modelling. *Aust. J. Earth Sci.* 66, 37–45. <https://doi.org/10.1080/08120099.2018.1525783>
- King, T.R., Quigley, M.C., Clark, D., 2018. Earthquake environmental effects produced by the Mw 6.1, 20th May 2016 Petermann earthquake, Australia. *Tectonophysics* 747–748, 357–372. <https://doi.org/10.1016/j.tecto.2018.10.010>
- Korsch, R.J., Goleby, B.R., Leven, J.H., Drummond, B.J., 1998. Crustal architecture of central Australia based on deep seismic reflection profiling. *Tectonophysics* 288, 57–69. [https://doi.org/10.1016/S0040-1951\(97\)00283-7](https://doi.org/10.1016/S0040-1951(97)00283-7)

- Lambeck, K., Burgess, G., 1992. Deep crustal structure of the musgrave block, central australia: Results from teleseismic travel-time anomalies. *Aust. J. Earth Sci.* 39, 1–19. <https://doi.org/10.1080/08120099208727996>
- Leonard, M., 2008. One hundred years of earthquake recording in Australia. *Bull. Seismol. Soc. Am.* 98, 1458–1470. <https://doi.org/10.1785/0120050193>
- Magee, J.W., 2009. Palaeovalley Groundwater Resources in Arid and Semi-Arid Australia A Literature Review Palaeovalley Groundwater Resources in Arid and Semi-Arid Australia - A literature review.
- Michetti, A.M., Esposito, E., Guerrieri, L., Porfido, S., Serva, L., Tatevossian, R.E., Vittori, E., Audemard M., F.A., Azuma, T., Clague, J., Comerci, V., Gурpinar, A., McCalpin, J.P., Mohammadioun, B., Morner, N.A., Ota, Y., Roghoshin, E., 2007. Intensity Scale ESI 2007, *Memorie Descrittive della Carta Geologica d'Italia, Special Volume 74*. APAT, Rome 2007.
- Neumann, N.L., 2013. Yilgarn Craton – Officer Basin – Musgrave Province Seismic and MT Workshop (GA Record 2013/28). Geoscience Australia, Commonwealth of Australia, Canberra, ACT. <https://doi.org/http://pid.geoscience.gov.au/dataset/ga/76664>
- Polcari, M., Albano, M., Atzori, S., Bignami, C., Stramondo, S., Polcari, M., Albano, M., Atzori, S., Bignami, C., Stramondo, S., 2018. The Causative Fault of the 2016 Mwp 6.1 Petermann Ranges Intraplate Earthquake (Central Australia) Retrieved by C- and L-Band InSAR Data. *Remote Sens.* 10, 1311. <https://doi.org/10.3390/rs10081311>
- Quigley, M.C., Mohammadi, H., Duffy, B.G., 2017. Multi-fault earthquakes with kinematic and geometric rupture complexity : how common ? INQUA Focus Group Earthquake Geology and Seismic Hazards.
- Raimondo, T., Collins, A.S., Hand, M., Walker-Hallam, A., Smithies, R.H., Evins, P.M., Howard, H.M., 2010. The anatomy of a deep intracontinental orogen. *Tectonics* 29. <https://doi.org/10.1029/2009TC002504>
- Scrimgeour, I.R., Close, D.F., Edgoose, C.J., 1999a. Petermann Ranges SG52-7; explanatory notes. Northern Territory Geological Survey, Darwin, Australia.
- Scrimgeour, I.R., Close, D.F., Edgoose, C.J., 1999b. Petermann Ranges 1:250 000 geological map, Second Edition. Northern Territory Geological Survey, Darwin, Australia.
- Somerville, P.G., Irikura, K., Graves, R.W., Sawada, S., Wald, D.J., Abrahamson, N.A., Iwasaki, Y., Kagawa, N., Smith, N.F., Kowada, A., 1999. Characterizing earthquake slip models for the prediction of strong ground motion. *Seismol. Res. Lett.* 70, 59–80.
- Stewart, A.J., 1995. Western extension of the Woodroffe Thrust, Musgrave Block, central Australia. *AGSO J. Aust. Geol. Geophys.* 16, 147–153.
- Wade, B.P., Kelsey, D.E., Hand, M., Barovich, K.M., 2008. The Musgrave Province: Stitching north, west and south Australia. *Precambrian Res.* 166, 370–386. <https://doi.org/10.1016/j.precamres.2007.05.007>
- Wang, S., Xu, W., Xu, C., Yin, Z., Bürgmann, R., Liu, L., Jiang, G., 2019. Changes in Groundwater Level Possibly Encourage Shallow Earthquakes in Central Australia: The 2016 Petermann Ranges Earthquake. *Geophys. Res. Lett.* 46, 3189–3198. <https://doi.org/10.1029/2018GL080510>
- Wex, S., Mancktelow, N.S., Camacho, A., Pennacchioni, G., 2019. Interplay between seismic fracture and aseismic creep in the Woodroffe Thrust, central Australia – Inferences for the rheology of relatively dry continental mid-crustal levels. *Tectonophysics* 758, 55–72. <https://doi.org/10.1016/j.tecto.2018.10.024>